Spin Sublevel Selectivity in Radiative and Non-Radiative Processes of the Lowest Excited Triplet State of 2,2′-Bipyridine

Takeshi Ikeyama*

Department of Chemistry, Miyagi University of Education, Sendai 980-0845, Japan

Noriyuki Okabe and Tohru Azumi†

Department of Chemistry, Faculty of Science, Tohoku University, Sendai 980-8578, Japan

Received: December 31, 2000; In Final Form: May 9, 2001

The spin sublevel properties (total decay rate constants k_i, relative radiative decay rate constants k_i^r of each vibronic bands in the phosphorescence spectrum, relative spin sublevel selectivity of the $S_1 \sim T_1$ intersystem crossing rates P_i, and relative steady-state populations N_i, where $i = x, y, z$ denote spin sublevels) of the lowest excited triplet state of 2,2′-bipyridine (bpy) doped in durene were observed with optical detection of microwave resonance (ODMR) spectroscopy. All of these parameters show that the two in-plane spin sublevels are active, in agreement with the group theoretical analysis assuming C_{2h} (trans-planar) configuration. The two in-plane components, which belong to the same character in C_{2h} point group, are distinguished on the basis of a calculation of the anisotropy of spin−orbit coupling matrix elements between $n\pi^*$ and $\pi\pi^*$ states and between $\sigma\pi^*$ and $\pi\pi^*$ states. The possible mechanisms of the $T_1 \rightarrow S_0$ radiative and $S_1 \sim T_1$ nonradiative processes are discussed.

Introduction

2,2′-Bipyridine (bpy), which has a torsional flexibility around the central C−C bond connecting the two pyridine rings, has been of interest in the structures in the ground and in the excited states. Many investigations on the structures of bpy have been presented both theoretically and experimentally.[1−4] Particularly on the lowest excited triplet state, the electronic and geometrical structures have been discussed from the viewpoint of the spin sublevel properties such as the zero field splitting constants (D and E), total decay rate constants (k_i), relative radiative decay rate constants (k_i^r), relative spin sublevel selectivity of $S_1 \sim T_1$ intersystem crossing rates (P_i), and relative steady-state populations (N_i). Experimental techniques that have been applied to this system are electron paramagnetic resonance (EPR),[3,5−6] time-resolved EPR (TR-EPR)[7], and optical detection of magnetic resonance (ODMR) spectroscopy.[4,8]

TR-EPR is a powerful tool to obtain the dynamical properties of the sublevels; however, the method gives us information only about the nonradiative processes of the $S_1 \sim T_1$ intersystem crossing rate (i.e., the populating rate). Moreover, concerning the populating rate, some uncertainty remains. The analysis of the signal gives only a ratio of the difference such as $(P_x - P_z)/(P_y - P_z)$. Therefore, the populating rates are usually obtained by assuming the smallest populating rate to zero, e.g., $P_z = 0$.

In the ODMR spectroscopy, on the other hand, the procedure to determine the populating rates is quite complicated, but the rates can be determined without any uncertainty. Further, other kinetic parameters can also be determined.

The ODMR measurements of the lowest excited triplet states of organic molecules were reported for the first time by Sharnoff,[9] Kwiram,[10] and Schmidt et al.[11] in 1967. In these early experiments the resonances were achieved by sweeping an external magnetic field. However, without an external magnetic field, the resonance signal can also be detected optically by sweeping the microwave frequency (the phosphorescence microwave double resonance (PMDR) method[12]). The zero-field nature of the ODMR experiment is suitable to determine the kinetic properties of the individual triplet spin-sublevel, and several experimental arrangements were proposed. The microwave-induced delayed phosphorescence (MIDP) measurement was proposed by Schmidt et al.[13−15] to determine the kinetic parameters relating to the triplet spin-sublevels. For the same purposes, a different transient method (the fast-passage method) was proposed by Winscom and Maki.[16]

On the application of the ODMR method to bpy, two papers have been reported:[4,8] one by Vinodgopal et al.[4] and the other by Suisalu et al.[8] Vinodgopal et al. classified the vibronic bands in the phosphorescence spectrum into two types according to the differences in the PMDR behavior. Some vibronic bands have negative 2E PMDR signals, whereas most of vibronic bands have positive PMDR signals on the 2E transition. These authors assigned the vibronic bands having negative PMDR signals as due to vibronic bands involving ungerade (i.e., a_u and b_u) vibrations. They further claimed that the appearance of these ungerade vibrations was the result of the molecular distortion from the planar configuration. We note, however, that such experimental findings can also be interpreted without assuming the molecular distortion, and therefore we need to investigate this behavior a little more carefully.

Suisalu et al. obtained the dynamic parameters, k_i, k_i^r, and N_i by the fast-passage method.[8] They concluded that the out-of-plane spin sublevel was the most active in the radiative

* To whom correspondence should be addressed. E-mail: t-ike@staff.miyakyo-u.ac.jp.

† Present address: Minnesota State University-Akita, 193-2 Okutzubakidai, Yuwa-machi, Akita 010-1211, Japan.

10.1021/jp0100856 CCC: $20.00
Published on Web 07/04/2001

transition. They further interpreted this result in terms of the distortion from planarity. However, as we discussed in a previous paper,[17] this analysis of the fast-passage signals are doubtful.

In this paper, we first of all determine the directions of the fine structure axes on the basis of angular dependence of the EPR signals and further reassign the vibronic bands in the phosphorescence spectrum on the basis of the ODMR results. Then, we discuss the radiative processes of the lowest excited triplet state and the nonradiative $S_1 \sim T_1$ processes. In the last section, we also show the results of theoretical calculations of the anisotropy of the spin−orbit couplings between $n\pi^*$ and $\pi\pi^*$ states and between $\sigma\pi^*$ and $\pi\pi^*$ states, and discuss the differences between two in-plane components in the radiative and nonradiative processes.

Experimental Section

Materials. The sample is a mixed crystal of 2,2′-bipyridine (bpy) doped in durene. Bpy was purified by recrystalization twice from ethanol and subsequent vacuum sublimation. Durene was purified by passing through an activated alumina column (*n*-pentane as solvent) and subsequent zone-melting (about 150 passes). A mixed crystal of bpy in durene was grown from the melt in a Bridgman furnace with the initial weight concentration of 1%.

Apparatus. EPR measurements were made by JEOL JES−FE2XGS EPR spectrometer. Phosphorescence spectrum was observed with a SPEX 1702 monochromator equipped with a HAMAMATSU R928 photomultiplier tube. A 500 W super high-pressure Hg arc was used as an excitation source. The ODMR measurements were carried out with a HP8690B sweep oscillator with an appropriate plug-in. Microwave was fed to a helix coil through coaxial cable. The data were recorded by an IWATSU DM-901 digital memory and averaged on a personal computer. All ODMR measurements were performed at zero-magnetic field and at 1.2 K where the spin−lattice relaxation is eliminated.

Measurements of the Spin-Sublevel Parameters. The fine structure axes were determined by analyzing angular dependence of the EPR signals.[18] The total decay rate constants (k_i, where $i = x, y, z$ denote the spin sublevels) and radiative decay rate constants (k_i^r) of the individual vibronic bands were determined by the combination of two types of ODMR methods: the microwave induced delayed phosphorescence (MIDP) method[15] and the fast-passage method.[16] In this way, we remove the uncertainty of the fast-passage simulations discussed in a previous paper.[17]

To determine the relative steady-state populations (N_i) and relative populating rates (P_i) for the *i*th sublevel, we used the relative radiative decay rate constants (k_i^r) of the 0−0 band, total decay rate constants (k_i), and the phosphorescence decay from the steady-state populations of three spin sublevels under the condition of spin polarization. To establish the steady-state populations, excitation with 20 s duration was carried out. The phosphorescence decay under the condition of spin polarization is expressed as

$$I(t) = \sum_{i=x,y,z} N_i k_i^r \exp(-k_i t)$$

Therefore, the nonlinear least-squares fit assuming three exponential decays with total decay rate constants provide N_i. The time evolution of the population of a spin sublevel, which equals 0 under steady-state condition, is expressed as

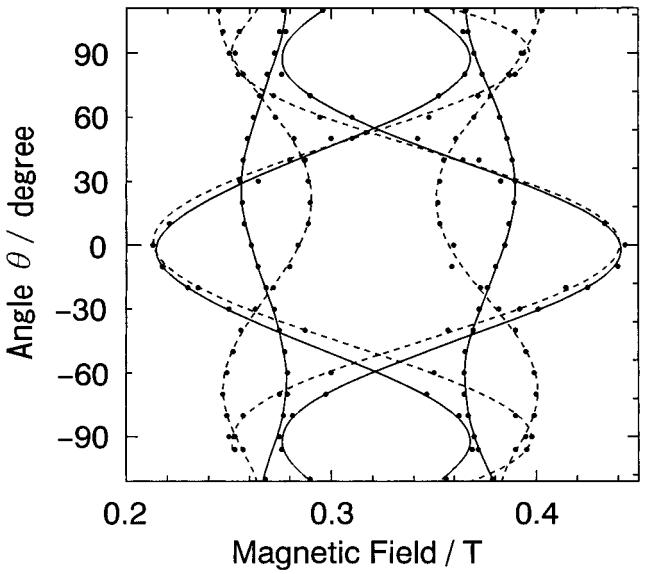

Figure 1. Angular dependence of the resonant magnetic field of EPR of 2,2′-bipyridine doped in durene observed at 77 K: experimental results (- - -) and best fit results (—) for two sites (shown in Figure 2). θ is an angle between the external magnetic field and the long axis (*L*) of durene in one site and is changed in the *a*−*b* plane of durene crystal.

$$\frac{dN_i}{dt} = P_i - N_i k_i = 0$$

Then, the relative populating rates, P_i, are calculated from the k_i and N_i values.

Results and Discussion

Assignment of Spin Axes. The angular dependence of the resonant field of the EPR of 2,2′-bipyridine (bpy) observed at 77 K (- - -), and the best fit results (—) are shown in Figure 1. The results clearly show the existence of four sites. Bpy is known to have (*E*)-conformation in solutions[19] and in the crystaline state.[2] The origins of four sites are reasonably understood by the fact that two different sites exist in the durene single crystal[20] and (*E*)-bpy in each site has two possible orientations as to the position of nitrogen atoms.

Hyperfine splitting of two hydrogen atoms is also observed with the intensity ratio 1:2:1. The hyperfine splitting observed reaches its maximum value at a direction of magnetic field parallel to the in-plane short axis (*M*) of durene. Calculation of spin density shows that the hydrogen atoms at 5 and 5′ positions cause the splitting. Then, the hyperfine splitting is expected to reach its maximum at a magnetic field that is perpendicular to both directions of the C5−H5 bond (which coincides with C5′−H5′ bond) and of 2p orbitals in the π system.[21] Therefore, the observed hyperfine splittings show that the direction of C5−H5 bond roughly coincides with the durene long axis (*L*).

The above two observations clearly indicate that bpy molecules go into the durene structure substitutionally with their molecular axes, at least approximately, parallel to those of the durene molecules. The direction of the spin axes of bpy was determined by analyzing the angular dependence of fine structures in Figure 1. The results are shown in Figure 2 as Eulerian angles between the molecular axes of durene (*L*, *M*, *N*) and the fine structure axes of bpy (*x*, *y*, *z*). The assignment of fine structure axes and direction of spin axes are shown in Figure 3, where the out-of-plane *z*-sublevel is placed lowest, as is expected theoretically for aromatic $^3\pi\pi^*$ states.[22]

As shown in Figure 2 the direction of the fine structure axis of the highest energy spin sublevel (*x*) deviates 20° from the

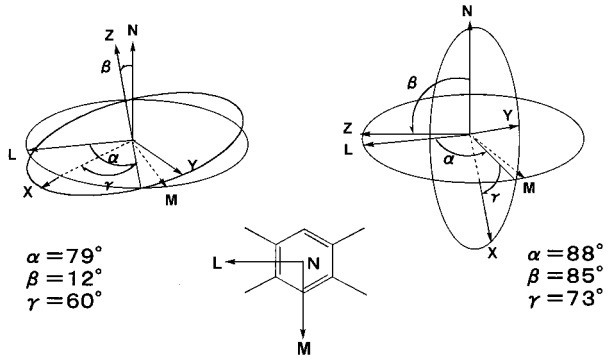

Figure 2. Eulerian angles between the molecular axes of durene (*L*, *M*, *N*) and fine structure axes (*x*, *y*, *z*) of 2,2′-bipyridine obtained by the simulation of the angular dependence of fine structures in Figure 1.

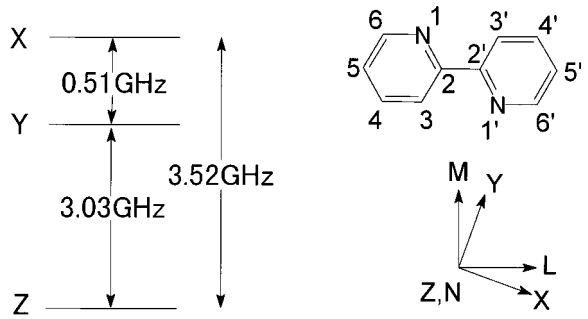

Figure 3. Assignment of three spin sublevels and direction of spin axes of the lowest excited triplet state of 2,2′-bipyridine doped in durene.

long axis (*L*) of durene; and the axis of the lowest energy spin sublevel (*z*) deviates 12° from the out-of-plane axis (*N*) of durene. Molecular dimensions of bpy and durene are similar in the directions of the short-axis and the out-of-plane axis, but the long-axis of bpy is evidently longer than that of durene. Therefore, it is reasonable to expect that bpy in the durene host rotates around the short (*M*) axis of durene. Then, we conclude that the relative orientation of bpy to durene is as follows: (i) the direction of the short molecular axis of bpy coincides with that of durene; (ii) the molecular plane of bpy makes an angle 12° to the plane of durene; and (iii) the angle between the *x*-spin axis of bpy and the *L*-axis of durene is 20° when rotating around the *N*-axis.

One uncertainty remains on the direction of spin axes. Though a spin axis is revealed to make an angle of 20° to the *L*-axis of durene, that is, 20° to the long-molecular axis of bpy, it is not clear whether the 20° rotation is in the positive or negative direction toward the nitrogen atom. The reasonable direction is depicted in Figure 3 according to theoretical considerations on the radiative and nonradiative processes. The detailed discussion is given in a later section.

Assignments of Vibronic Bands in the Phosphorescence Spectrum. Figure 4 shows the high energy portion of the phosphorescence spectrum observed at 1.2 K. The relative radiative decay rate constants k_i^r observed for individual vibronic bands are also shown. In this figure, the vibronic structures are well resolved and are similar to those observed in a Shpol'skii matrix,[4] except for the 160 cm^{-1} band and its combination bands. The assignment of the vibronic structures in the phosphorescence spectrum of bpy in *n*-heptane was made by Vinodgopal et al. with the help of the sign of 2*E* PMDR signals.[4] These authors assigned the bands that showed the negative 2*E* PMDR signals to the vibronic bands involving ungerade vibrations (a_u or b_u). Furthermore, they concluded that the appearance of these forbidden bands is the result of distortion from the planarity. Our previous ODMR results,[17] however, indicated that the bpy takes a planar configuration. Further, the bands that were assigned to a_u and b_u vibronic bands seem to have intensities too large to assign as forbidden bands. With the arguments stated above, we rather assign these bands as allowed transitions involving b_g vibrations.

From the result of normal-mode analysis of the vibrations,[23,24] the lower energy nontotally symmetric vibrations are expected at 223 cm^{-1} b_g, 106 cm^{-1} a_u, and 160 cm^{-1} b_u, if these are active in the phosphorescence spectrum. Therefore, we first determine k_i^r for these vibronic bands and use the values as a standard to assign other vibronic bands. Experimentally, bands are observed at 230, 99, and 160 cm^{-1}. At the 230 cm^{-1} vibronic band, the *y*-spin sublevel is most radiative, in contrast to the

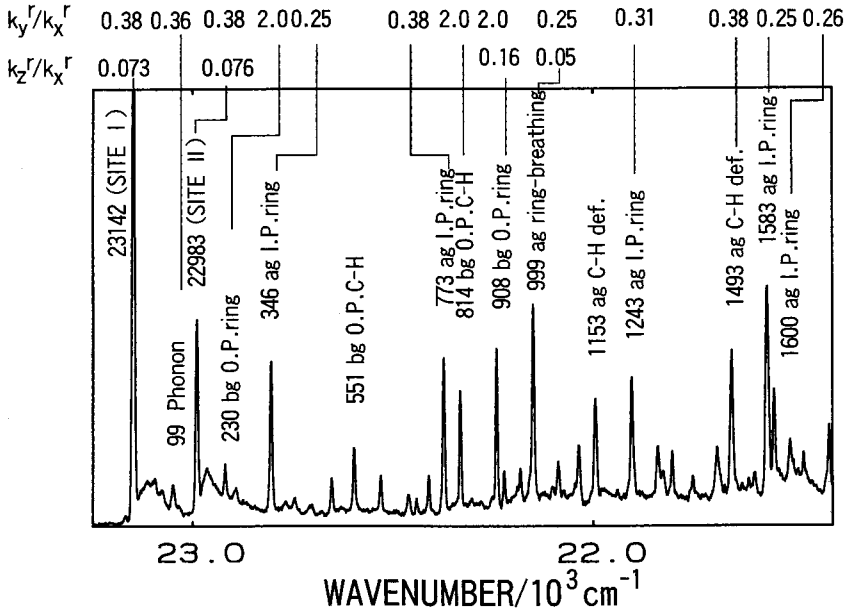

Figure 4. High-energy portion of the phosphorescence spectrum of 2,2′-bipyridine doped in durene at 1.2 K. The energy of the 0−0 band of site 1 and site 2 and the vibrational mode of the main vibronic bands are indicated. The assignments of the other weak peaks are listed in Table 1. The relative radiative decay rate constants of main vibronic bands are also indicated.

TABLE 1: Assignment of the Vibronic Structures of High Energy Portion of the Phosphorescence Spectrum of 2,2′-Bipyridine Doped in Durene at 1.2 K

energy/ cm^{-1}	Δenergy/ cm^{-1}	assignment[a]		
		this work	ref 4	
23142		site 1(0−0)		
23043	99	phonon	110	a_u
22983	159	site 2(0−0)		
22912	230	b_g(O. P. ring)		
22796	346	a_g(I. P. ring)	316	a_g
22693	449	b_g(O. P. ring)	439	b_g
22645	499	346 + 159		
22591	551	b_g(O. P. C−H)		
22525	617	a_g(I. P. ring)	608	a_g
22456	686	346 + 346	639	316 + 316
22436	706	551 + 159		
22406	736		717	b_g
22369	773	a_g(I. P.ring)	753	a_g
22328	814	b_g(O. P. C−H)	805	a_u
22234	908	b_g(O. P. ring)	882	b_u
22217	925	773 + 159		
22183	959	b_g(O. P.ring)		
22175	967	814 + 159		
22143	999	a_g(ring-breathing)	977	b_g
22086	1056	908 + 159		
22030	1112	a_g(I. P. ring)	1083	a_g
21989	1153	a_g(C−H def)	1119	a_g
21899	1243	a_g(I. P. ring)	1214	a_g
21834	1308	a_g(I. P. ring)	1288	a_g
21823	1319	a_g(C−H def)	1313	a_g
21799	1343	999 + 346		
21748	1394	1243 + 159		
21686	1456	a_g(C−H def)	1428	a_g
21649	1493	a_g(C−H def)	1459	a_g
			1532	1214 + 316
21559	1583	a_g(I. P. ring)	1565	
21542	1600	a_g(I. P. ring)	1585	a_g

[a] O. P., out-of-plane; I. P., in-plane; def, deformation.

0−0 band in which the *x*-spin sublevel is most radiative. This band is assigned to b_g symmetry.

On the other hand, we assign the band observed at 99 cm^{-1} not to an a_u vibronic band but to a phonon band, because the relative radiative decay rate constants are almost the same as those of the 0−0 band. Moreover, we assign the band observed at 160 cm^{-1} in the phosphorescence spectrum as a 0−0 transition of a different site (site 2) for the following reasons: (i) this band does not appear in Shpol'skii solvent (*n*-heptane); (ii) the existence of two sites is indicated also in the EPR result (Figure 1). We first assign the b_g vibronic bands in terms of k_i^r ratio and next assign the rest of the vibronic bands using the results of IR and Raman spectra.[23,25] The results of the assignment are listed in Table 1. The assignment differs somewhat from that of Vinodgopal et al.,[4] on the vibronic bands at 805, 882, and 77 cm^{-1}. They assigned these bands as a_u, b_u, and b_g, respectively; in contrast, we assigned b_g, b_g, and a_g, respectively. In our assignment, there are no a_u and b_u vibronic bands, which are expected to appear in the phosphorescence spectrum only if the C_{2h} trans-planar configuration is broken.

Assignment of the Lower Electronic States. In this section, we summarize the symmetries and energies of the lower electronic states for the discussion of the radiative and nonradiative processes. In the previous section, it is shown that the structure of bpy keeps a planar (*s*-trans) configuration: C_{2h} point group. From the result of an MO calculation[3] under the C_{2h} point group, the lowest excited triplet state is the $^3B_u(\pi\pi^*)$ state and the second triplet state is the $^3A_u(n\pi^*)$ or $^3B_g(n\pi^*)$ state. Therefore, the symmetries of the in-plane and out-of-plane spin-sublevels (space × spin) of the lowest excited triplet state are A_u and B_u, respectively. On the other hand, the lowest excited singlet state is the $^1B_g(n\pi^*)$ or $^1A_u(n\pi^*)$ state. The symmetry of the lowest excited singlet state is important for the discussion of the $S_1 \sim T_1$ nonradiative process. From the absorption spectrum of bpy doped in biphenyl,[24] the lowest excited singlet state is assigned to $^1B_g(n\pi^*)$, but from the result of ab initio calculation[3], it is assigned to the $^1A_u(n\pi^*)$ state. We will discuss this problem in a later section and conclude that the $^1B_g(n\pi^*)$ state is the lowest excited singlet state.

TABLE 2: Radiative Mechanisms of the 0−0 Band and Bands Involving a_g Vibrations

spin sublevel	mechanism[a]
	(A) First-Order
τ_x, τ_y	$^3B_u^{x,y}(\pi\pi^*) \frac{H_{SO}}{\text{1-center}} {}^1A_u(n\pi^*,\sigma\pi^*) \frac{er}{small} {}^1A_g$
τ_z	$^3B_u^{z}(\pi\pi^*) \frac{H_{SO}}{\text{3-center}} {}^1B_u(\pi\pi^*) \frac{er}{large} {}^1A_g$
	(B) Second-Order
τ_x, τ_y	$^3B_u^{x,y}(\pi\pi^*) \frac{H_{SO}}{\text{1-center}} {}^3A_u^{z}(n\pi^*,\sigma\pi^*) \frac{H_{SO}}{\text{1-center}} {}^1A_u(n\pi^*,\sigma\pi^*) \frac{er}{small} {}^1A_g$
τ_z	$^3B_u^{z}(\pi\pi^*) \frac{H_{SO}}{\text{1-center}} {}^3A_u^{x,y}(n\pi^*,\sigma\pi^*) \frac{H_{SO}}{\text{1-center}} {}^1B_u(\pi\pi^*) \frac{er}{large} {}^1A_g$

[a] H_{so}/1(or 3)-center, spin−orbit coupling involving one (or three) center atomic integrals; er, electric dipole coupling. The mechanism including three center atomic integral is shown only when the one center integral vanishes.

The energies of these states are estimated as follows: 23143 cm^{-1} for the lowest excited triplet state $^3B_u(\pi\pi^*)$ from the energy of the phosphorescence origin, 27000∼28000 cm^{-1} for the second triplet state $^3A_u(n\pi^*)$ or $^3B_g(n\pi^*)$ from the amount of exchange integral of usual $n\pi^*$ state of aromatic hydrocarbons and energies of corresponding singlet states, 30000∼30800 cm^{-1} for the lowest and the second excited singlet states $^1B_g(n\pi^*)$ and $^1A_u(n\pi^*)$ from the absorption spectrum of bpy doped in biphenyl,[24] and about 33000 cm^{-1} for the third excited singlet state $^1B_u(\pi\pi^*)$.

The Radiative Mechanism of the 0−0 Band. Relative radiative decay rate constants of the 0−0 band (Figure 4) show the following two remarkable features: (i) the in-plane *x*-spin sublevel is most active and (ii) the out-of-plane *z*-spin sublevel is the smallest but rather active ($k_z^r/k_x^r = 0.07$) in comparison with the usual aza-aromatic hydrocarbons (e.g., for quinoxaline,[15] $k_z^r/k_x^r = 0.013$).

The mechanism in which the 0−0 band gains intensity is the direct spin−orbit coupling mechanism as shown in Table 2, part A. From this information, in-plane spin sublevels are expected to be more active than the out-of-plane spin sublevel. This expectation coincides well with the experimental result that the out-of-plane *z* is the least emissive (the fore part of the above feature (ii)). Therefore, bpy is indicated to have a planar π configuration as discussed in the previous paper.[17]

The reason why the out-of-plane spin sublevel is slightly active in bpy is explained as a contribution from a second-order perturbation term shown in Table 2, part B. In quinoxaline, the direction of one fine structure axis coincides with the direction of nonbonding orbital of nitrogen.[15] Let *y* be the spin axis that has the same direction with nonbonding orbital p_N of nitrogen,

then the atomic integral $\langle p_N|\xi L_y|p_z\rangle$ in the expression of the matrix element H_{SO} is zero in one-center approximation. The situation makes one of the spin−orbit coupling terms in Table 2B vanish, and the contribution of the second-order mechanism disappears. In bpy, on the other hand, the direction of any fine structure axis does not coincide with the direction of nonbonding orbital of nitrogen. Therefore, the contribution from the second-order perturbation terms remains and makes the out-of-plane spin sublevel slightly active.

Another possibility that the out-of-plane spin sublevel gains intensity is a distortion from planarity. A distortion from planarity, such as a torsion between two pyridines, introduces σ-type character into π orbitals. The introduced σ-type character in π orbitals makes the one-center integral of spin−orbit coupling matrix element between π orbitals nonzero relative to the out-of-plane spin sublevel. However, from the results in previous sections, i.e., there is no indication of a_u and b_u vibronic bands in the phosphorescence spectrum, the possibility of a geometry distortion is eliminated.

The Radiative Mechanism of the Bands Involving a_g Vibration. In principle the radiative mechanism of the bands involving a_g vibration is the same as that of the 0−0 band shown in Table 2, so relative radiative decay rate constants are expected to be the same as that of the 0−0 band. However, detailed analysis of the experimental results shows some vibrational mode dependence of the relative radiative decay rate constants. The a_g vibronic bands (i.e., 345, 999, 1586, and 1591 cm^{-1}) show $k_y^r/k_x^r = 0.25-0.26$; 0−0 band and the 773 and 1497 cm^{-1} vibronic bands show $k_y^r/k_x^r = 0.38$. The mode dependence is remarkable in skeletal vibrations. Similar mode dependence has been reported in the skeletal vibrations of tetrachlorobenzene[26] and pyrazine.[27] This type of vibrational mode dependence has been explained as the breakdown of the Condon approximation.

The Radiative Mechanism of the Bands Involving b_g Vibration. As shown in Figure 4, the in-plane *y*-spin sublevel is most radiative in the bands involving b_g vibrations; in contrast, the in-plane *x*-spin sublevel is most radiative in the 0−0 band and the bands involving a_g vibrations.

The bands involving b_g vibrations acquire intensity through the spin−orbit coupling with the vibronic coupling in the singlet and/or triplet manifolds. The mechanisms of radiative processes of the bands involving b_g vibrations are shown in Table 3. From this information, it is shown that vibronic couplings in both singlet and triplet manifolds make the in-plane spin sublevels more active than the out-of-plane one, which is consistent with the experimental results. The differences in the two in-plane spin sublevels are discussed in the last section.

Spin Sublevel Selectivity of $S_1 \sim T_1$ Intersystem Crossing Rates. In Table 4, we show the parameters of relative spin sublevel selectivity of $S_1 \sim T_1$ intersystem crossing rates P_i (populating rate), and relative steady-state populations N_i determined by ODMR spectroscopy. The populating rates were first observed by Yagi et al. with TR-EPR spectroscopy.[7] TR-EPR is a powerful tool to obtain the spin sublevel properties, but this method has some difficulties as stated in the Introduction. In bpy, however, the difficulty is not so serious because bpy keeps trans-planar configuration in the lowest excited triplet state. Therefore, the ratio $(P_x - P_z)/(P_y - P_z)$, determined with TR-EPR, coincides well with that determined with ODMR.

From Table 4, it is clear that the in-plane *y*-spin sublevel is the most active in the $S_1 \sim T_1$ nonradiative process. The mechanism of the nonradiative process was first discussed by

TABLE 3: Radiative Mechanisms of the Bands Involving b_g Vibrations

spin sublevel	mechanism[a]
	(A) Vibronic Coupling in the Singlet Manifold
τ_x, τ_y	$^3B_u^{x,y}(\pi\pi^*) \xrightarrow{H_{SO}/\text{1-center}} {}^1A_u(n\pi^*,\sigma\pi^*) \xrightarrow{H_{vib}/b_g} {}^1B_u(\pi\pi^*) \xrightarrow{er/\text{large}} {}^1A_g$
τ_z	$^3B_u^{z}(\pi\pi^*) \xrightarrow{H_{SO}/\text{3-center}} {}^1B_u(\pi\pi^*) \xrightarrow{H_{vib}/b_g} {}^1A_u(n\pi^*,\sigma\pi^*) \xrightarrow{er/\text{small}} {}^1A_g$
	(B) Vibronic Coupling in the Triplet Manifold
τ_x, τ_y	$^3B_u^{x,y}(\pi\pi^*) \xrightarrow{H_{vib}/b_g} {}^3A_u^{x,y}(n\pi^*,\sigma\pi^*) \xrightarrow{H_{SO}/\text{1-center}} {}^1B_u(\pi\pi^*) \xrightarrow{er/\text{large}} {}^1A_g$
τ_z	$^3B_u^{z}(\pi\pi^*) \xrightarrow{H_{vib}/b_g} {}^3A_u^{z}(n\pi^*,\sigma\pi^*) \xrightarrow{H_{SO}/\text{1-center}} {}^1A_u(n\pi^*,\sigma\pi^*) \xrightarrow{er/\text{small}} {}^1A_g$

[a] H_{so}/1(or 3)-center, spin−orbit coupling involving one (or three) center atomic integrals; H_{vib}/b_g, vibronic coupling through b_g vibrational mode; er, electric dipole coupling. The mechanism including three center atomic integral is shown only when the one center integral vanishes.

TABLE 4: Relative $S_1 \sim T_1$ Intersystem Crossing Rates P_i and the Relative Steady-State Populations N_i of the Lowest Excited Triplet State of 2,2′-Bipyridine Doped in Durene

spin sublevel	P_i(rel)	N_i(rel)
τ_x	1.00	1.00
τ_y	5.23	3.25
τ_z	0.44	2.26

Yagi et al.[7] by assuming two possible states $^1B_g(n\pi^*)$ and $^1A_u(n\pi^*)$ as initial states (i.e., the lowest excited singlet state). They proposed that $^1A_u(n\pi^*)$ is more probable as the lowest excited singlet state on the basis of ab initio calculation.[3] Following their considerations, the in-plane spin sublevels are more active than the out-of-plane sublevel in the two initial states.[28] This expectation agrees well with the experimental results. In Table 5, we show the mechanisms of $S_1 \sim T_1$ nonradiative process following Yagi et al. In the next section, we further discuss the initial state in $S_1 \sim T_1$ nonradiative process on the basis of the calculation of spin−orbit coupling matrix elements.

Differences in the Two In-Plane Spin Sublevels. In the previous sections, the differences between the in-plane and out-of-plane spin sublevels are analyzed with group theoretical considerations. The analysis explains the experimental results very well. However, the experimental results of ODMR indicate clear differences also between two in-plane spin sublevels. For example, of the relative radiative decay rate constants k_i^r of the 0−0 band and bands involving a_g vibrations, the in-plane *x*-spin sublevel is more active than the in-plane *y*-spin sublevel, but the k_i^r of the bands involving b_g vibrations and the spin-sublevel selectivity in the $S_1 \sim T_1$ nonradiative process P_i, the *y*-spin sublevel, is more active than the *x*-spin sublevel. The difference cannot be explained only by group theoretical considerations because under the C_{2h} point group the two in-plane spin

TABLE 5: Mechanism of $S_1 \sim T_1$ Nonradiative Transition

spin sublevel	mechanism[a]
	(A) $S_1 = {}^1B_g(n\pi^*)$
τ_x, τ_y	${}^1B_g(n\pi^*)\,\frac{H_{vib}}{b_u}\,{}^1A_u(n\pi^*,\sigma\pi^*)\,\frac{H_{SO}}{1\text{-center}}\,{}^3B_u{}^{x,y}(\pi\pi^*)$
	${}^1B_g(n\pi^*)\,\frac{H_{SO}}{1\text{-center}}\,{}^3A_g{}^{x,y}(\pi\pi^*)\,\frac{H_{vib}}{b_u}\,{}^3B_u{}^{x,y}(\pi\pi^*)$
τ_z	${}^1B_g(n\pi^*)^b\,\frac{H_{SO}}{1\text{-center}}\,{}^3B_g{}^z(n\pi^*,\sigma\pi^*)^b\,\frac{H_{vib}}{a_u}\,{}^3B_u{}^z(\pi\pi^*)$
	(B) $S_1 = {}^1A_u(n\pi^*)$
τ_x, τ_y	${}^1A_u(n\pi^*)\,\frac{H_{SO}}{1\text{-center}}\,{}^3B_u{}^{x,y}(\pi\pi^*)$
τ_z	${}^1A_u(n\pi^*)^c\,\frac{H_{SO}}{1\text{-center}}\,{}^3A_u{}^z(n\pi^*,\sigma\pi^*)^c\,\frac{H_{vib}}{b_g}\,{}^3B_u{}^z(\pi\pi^*)$

[a] H_{so}/1-center, spin−orbit coupling involving one center atomic integrals; H_{vib}/b_u, vibronic coupling through b_u vibrational mode; er, electric dipole coupling. [b] The singlet and the triplet $B_g(n\pi^*)$ states have different electronic configuration. [c] The singlet and the triplet $A_u(n\pi^*)$ states have different electronic configurations.

sublevels belong to the same symmetry species. To understand these differences, we must consider the matrix elements relating to the radiative and nonradiative processes, especially the anisotropy of the spin−orbit coupling matrix elements that give a strong perturbation to the spin sublevel selectivity of the intersystem crossing processes of the excited triplet states.

The spin−orbit coupling matrix elements between the singlet state $S_i(a,c)$ and triplet state $T_j(b,c)$ can be written by the molecular orbital (MO) description as follows:

$$\langle S_i(a,c)|H_{so}|T_j(b,c)\rangle = -\frac{1}{2}\hbar\langle\Phi_a|\xi(r)\cdot L_u|\Phi_b\rangle \qquad (1)$$

where a, b, c are the notation of MOs, L is the angular momentum of the molecule, u denotes the spin sublevel, and ξ is the spin−orbit coupling constant of the molecule. Φ_a and Φ_b are the following σ-type and π-type MOs, respectively:

$$\Phi_a = \sum_r (C_{sr}\chi_{sr} + C_{xr}\chi_{xr} + C_{yr}\chi_{yr}) \qquad (2)$$

$$\Phi_b = \sum_r C_{zr}\chi_{zr} \qquad (3)$$

where C is the coefficient of atomic orbitals, s means s-type atomic orbital, and x, y, z represent $2p_x$, $2p_y$, $2p_z$-type atomic orbitals, respectively. By expanding the MOs Φ_a and Φ_b into atomic orbitals χ, the matrix element in eq 1 is written as follows:

$$= -\frac{1}{2}\hbar(r)\sum_r\sum_s\sum_t\{C_{zr}C_{ys}\langle\chi_{zr}|\xi(r)\,L_{xt}|\chi_{ys}\rangle + C_{zr}C_{xs}\langle\chi_{zr}|\xi(r)\,L_{yt}|\chi_{xs}\rangle\} \qquad (4)$$

In this formula, r, s, t are notation of atoms. Moreover, this formula can be rewritten with the spin−orbit coupling parameter ζ, under the assumption that one-center integral (r = s = t) is dominant:

$$= -\frac{1}{2}\hbar(r)\sum_{r=s=t}\{C_{zr}C_{yr}\xi_{21r} + C_{zr}C_{xr}\xi_{21r}\} \qquad (5)$$

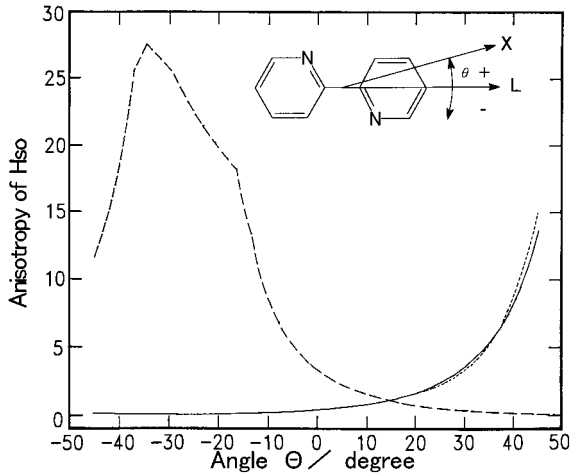

Figure 5. Calculated angular dependence of the anisotropy of the spin−orbit coupling matrix elements ($<|H_{SO}|>_y^2/<|H_{SO}|>_x^2$) between the $n\pi^*$ and $\pi\pi^*$ states and between the $\sigma\pi^*$ and $\pi\pi^*$ states: solid line, between $A_u(n\pi^*)$ and $B_u(\pi\pi^*)$ states; dotted line, between $B_g(n\pi^*)$ and $B_u(\pi\pi^*)$ states; broken line, between $A_u(\sigma\pi^*)$ and $B_u(\pi\pi^*)$ states. θ is an angle between the x-spin axis and the C−C bond binding two pyridines. The negative value of θ corresponds to the direction of rotation which makes x-spin axis approaching to the nitrogen atoms.

The first term in eq 5 contributes to the x-spin sublevel and the second term contributes to the y-spin sublevel. Then, we can calculate the anisotropy of spin−orbit coupling matrix elements with the value of ζ and LCAO-type MOs. For the purpose of this calculation, we used ζ reported by Blume et al.,[29] and the LCAO-type MOs obtained by the ab initio calculation with the STO-3G basis set.

The results of the calculation on the anisotropy of spin−orbit coupling matrix elements are shown in Figure 5. If the angle between the x-spin axis and the molecular long axis of bpy is known, the anisotropy of spin−orbit coupling matrix element between x and y spin-sublevels is read from this figure. As discussed in the previous sections, EPR measurements show that the angle between the x-spin axis and the L-axis of durene is about 20°. From Figure 5, if the rotation is positive (+20°), the anisotropies of spin−orbit coupling for x and y spin sublevels are minimal for both couplings between $n\pi^*$ and $\pi\pi^*$ states and between $\sigma\pi^*$ and $\pi\pi^*$ states. Then, the observed sublevel dependence cannot be explained. On the other hand, if the rotation is in the negative direction (−20°), x-spin sublevel is dominant in the spin−orbit coupling between $n\pi^*$ and $\pi\pi^*$ states (the anisotropy $<|H_{SO}|>_y^2/<|H_{SO}|>_x^2$ is 0.1) and the y-spin sublevel is dominant between the $\sigma\pi^*$ and $\pi\pi^*$ states ($<|H_{SO}|>_y^2/<|H_{SO}|>_x^2$ is 20). Therefore, we conclude that the rotation is negative as shown in Figure 3.

Experimental results show that the x-spin sublevel is most active in the radiative transition of the 0−0 band and the bands involving a_g vibrations (Figure 4). From the above considerations, these bands are expected to gain intensity through $n\pi^*$ states. Then, in the first-order radiative mechanisms in Table 2, the path through the $^1A_u(n\pi^*)$ state is probable. On the other hand, the radiative transitions of the bands involving b_g vibration gain intensity mainly through the paths of $\sigma\pi^*$ states. Therefore, in Table 3, the paths through the $^{1,3}A_u(\sigma\pi^*)$ states are most probable.

The results of the $S_1 \sim T_1$ nonradiative process indicate spin−orbit coupling with $\sigma\pi^*$ states. Therefore, in Table 5, the paths through the $^{1,3}A_u(\sigma\pi^*)$ states are most probable. This result indicates that the lowest excited singlet state, which is the initial state of the nonradiative transition, is the $^1B_g(n\pi^*)$ state, because,

if $^1A_u(n\pi^*)$ state is the lowest, the path of $^1A_u(n\pi^*)-H_{SO}-{}^3B_u(\pi\pi^*)$ is the main path which activate *x*-spin sublevel. On the other hand, the direct mechanism is forbidden in $^1B_g(n\pi^*)$ state. Then, the indirect mechanism through the excited $^1A_u(\sigma\pi^*)$ state is the main path and activate *y*-spin sublevel, which agrees with the experimental results.

One question exists about the above nonradiative mechanism. If the lowest singlet state is $^1B_g(n\pi^*)$, a path through $^1A_u(n\pi^*)$, which is energetically favorable, should also be possible additionally to the main path through $^1A_u(\sigma\pi^*)$. The path of $^1A_u(n\pi^*)$ activates the *x*-spin sublevel contrary to the $\sigma\pi^*$ states. A possible explanation is as follows: the anisotropy between $\sigma\pi^*$ and $\pi\pi^*$ states indicated in Figure 5 is larger than that between the $n\pi^*$ and $\pi\pi^*$ states; then, it cancels the disadvantage of the energy denominator.

Conclusion

In this report, we observed spin-sublevel properties of the lowest excited triplet state by ODMR spectroscopy and discussed the mechanisms of radiative and nonradiative processes. All sublevel properties are well explained by the trans-planar (C_{2h}) configuration; that is, nonplanar distortion is not present in bpy. With the result of calculations on anisotropy of spin−orbit coupling matrix elements, the differences in the two in-plane spin-sublevels, which are indistinguishable by group theoretical analysis, are clarified.

Acknowledgment. We thank Prof. S. Yamauchi and Prof. M. Iwaizumi, Institute for Chemical Reaction Science, Tohoku University, for their help in EPR measurements and discussions.

References and Notes

(1) Galasso, V.; De Alti, G.; Bigotto, A. *Tetrahedron* **1971**, *27*, 991.
(2) Merritt, L. L. Jr.; Schroeder, E. D. *Acta Crystallogr*. **1956**, *9*, 801.
(3) Yagi, M.; Makiguchi, K.; Ohnuki, A.; Suzuki, K.; Higuchi, J. *Bull. Chem. Soc. Jpn.* **1985**, *58*, 252.
(4) Vinodgopal, K.; Leenstra, W. R. *J. Phys. Chem.* **1985**, *89*, 3824.
(5) Gondo, Y.; Maki, A. H. *J. Phys. Chem.* **1968**, *72*, 3215.
(6) Higuchi, J.; Yagi, M.; Iwaki, T.; Bunden, M.; Taniguchi, K.; Ito, T. *Bull. Chem. Soc. Jpn.* **1980**, *53*, 890.
(7) Yagi, M.; Deguchi, Y.; Shioya, Y.; Higuchi, J. *Chem. Phys. Lett.* **1988**, *144*, 412.
(8) Suisalu, A. P.; Kamyshnyi, A. L.; Zakharov, V. N.; Aslanov, L. A.; Avarmaa, R. A. *Chem. Phys. Lett.* **1987**, *134*, 617.
(9) Sharnoff, M. *J. Chem. Phys.* **1967**, *46*, 3263.
(10) Kwiram, A. L. *Chem. Phys. Lett.* **1967**, *1*, 272.
(11) Schmidt, J.; Hesselmann, I. A. M.; de Groot, M. S.; van der Waals, J. H. *Chem. Phys. Lett.* **1967**, *1*, 434.
(12) Tinti, D. S.; El-Sayed, M. A.; Maki, A. H.; Harris, C. B. *Chem. Phys. Lett.* **1969**, *3*, 343.
(13) Schmidt, J.; Veeman, W. S.; van der Waals, J. H. *Chem. Phys. Lett.* **1969**, *4*, 341.
(14) Antheunis, D. A.; Schmidt, J.; van der Waals, J. H. *Chem. Phys. Lett.* **1970**, *6*, 255.
(15) Schmidt, J.; Antheunis, D. A.; van der Waals, J. H. *Mol. Phys.* **1971**, *22*, 1.
(16) Winscom, C. J.; Maki, A. H. *Chem. Phys. Lett.* **1971**, *12*, 264.
(17) Okabe, N.; Ikeyama, T.; Azumi, T. *Chem. Phys. Lett*. **1990**, *165*, 24.
(18) Hutchison, C. A., Jr.; Mangum, B. W. *J. Chem. Phys.* **1961,** *34*, 908.
(19) Nakamoto, K. *J. Phys. Chem.* **1960**, *64*, 1420. Castellano, S.; Günter, H.; Ebersole, S. *J. Phys. Chem.* **1965**, *69*, 4166.
(20) Robertson, J. M. *Proc. R. Soc. London A* **1933**, *142*, 659.
(21) McConnell, H. M.; Heller, C.; Cole, T.; Fessenden, R. W. *J. Am. Chem. Soc.* **1960**, *82*, 766.
(22) El-Sayed, M. A. In *Excited States 1*; Lim, E. C., Ed.; Academic Press: New York, 1974; p 35.
(23) Neto, N.; Muniz-Miranda, M.; Angeloni, L.; Castellucci, E. *Spectrochim. Acta* **1983**, *39A*, 97.
(24) McAlpine, R. D. *J. Mol. Spectrosc.* **1979**, *38*, 441.
(25) Castellucci, E.; Angeloni, L.; Neto, N.; Sbrana, G. *Chem. Phys.* **1979**, *43*, 365.
(26) Breiland, W. G.; Harris, C. B. *Chem. Phys. Lett.* **1973**, *18*, 309.
(27) Kokai, F.; Azumi, T. *J. Chem. Phys*. **1981**, *75*, 1069.
(28) In Table 5A, nonradiative processes of both out-of-plane and in-plane spin sublevels are the same in perturbation order, but the energy denominator of out-of-plane process is larger than that of in-plane, because the spin−orbit coupling matrix element between the same configuration vanishes. Therefore, the $^1B_g(n\pi^*)$ and $^3B_g(n\pi^*)$ states shown in τ_Z nonradiative process in Table 5A must have different electronic configurations. The situation is also similar in cases of Table 5B.
(29) Bethe, H. A.; Salpeter, E. E. *Quantum Mechanics of One- and Two-electron Atoms*; Springer-Verlag: Berlin, 1957; p 185.